Vacuum Magnetic Force Microscopy at High Temperatures: Observation of Permanent Magnets

Takehiro Yamaoka[1]*, Hana Tsujikawa[1], Satoshi Hasumura[1], Kazunori Andou[1], Masatsugu Shigeno[1], Akira Ito[2], and Hiroshi Kawamura[2]

[1]Hitachi High-Tech Science Corporation, 2-15-5 Shintomi, Chuo-ku, Tokyo 104-0041, Japan
[2]Nitto Optical Co., Ltd., Nitto Bldg., 1-14-18 Kudankita, Chiyoda-ku, Tokyo 102-0073, Japan

*yamaoka-takehiro@hhs.hitachi-hitec.com

Introduction

Magnetic materials are found in a range of applications, including electric appliances, quantum devices, data storage devices, automobiles, and generators. The increasing demand for electric vehicles has prompted the development of highly efficient permanent magnet motors that are free of the rare earth element dysprosium (Dy) and have a high heat resistance. In addition, recently there has been intense research on nanomagnetism along with advances in spintronics. Precise control and accurate observation of magnetization structures will be key components in future research and development.

Observation of magnetic domain structures can be undertaken using light, electron beams, or magnetic force microscopy (MFM) [1], a type of scanning probe microscopy (SPM). In MFM, a magnetic probe is scanned over the surface of the sample, and the magnetic interactions between the probe and sample are detected. Owing to the relatively simple sample preparation and small size of the apparatus, MFM has become widely employed, but MFM is not suitable for all kinds of ferromagnetic samples. For example, the stray magnetic field of the MFM probe may disturb magnetic domain structures in soft magnetic samples or nanoscale magnetic patterns. Saitoh et al. [2] and Yamaoka et al. [3] have succeeded in observing a single magnetic domain wall of almost no coercivity by weakening the stray magnetic field of the probe and implementing control of the quality factor (Q) in vacuum MFM. This technique has contributed to magnetic structure analysis of various nanoscale magnetic samples and high-density recording media [4, 5]. Accurate observations of magnetic domain structures in permanent magnets are also difficult because the large stray magnetic fields of the magnets disturb the magnetization of the MFM probe. This problem can be solved by using an MFM probe that has a coercivity 10 times stronger than that of conventional probes [6, 7]. This article reports precise magnetic domain observations of Nd-Fe-B permanent magnets by using a high-coercivity MFM probe and vacuum MFM observations of the thermal demagnetization of Nd-Fe-B magnets from room temperature to 400 °C.

Materials and Methods

High-coercivity probe. Stray magnetic fields of permanent magnets or strong external magnetic fields applied when conducting *in situ* observations affect the magnetic field of the MFM probe and result in images that are difficult to interpret. A high-coercivity MFM probe can prevent or minimize these effects, and an $L1_0$-type FePt ordered alloy with a large uniaxial crystal magnetic anisotropy is an effective probe material. Joint research by Akita University and Nitto Optical resulted in such a probe with a coercivity H_c that exceeded 10 kOe (1 Oe = 79.57 A/m) [8], and the same probe was used in this research. To fabricate the probe, the surface of a Si cantilever (spring constant of ~40 N/m; resonance frequency of ~250 kHz) was oxidized with a plasma (3 nm-thick SiO_2 film) and then coated with a 25 nm-thick FePt alloy. Figure 1a shows the magnetization–magnetic-field (M–H) loop of the conventional Co alloy thin film used for typical MFM probe coatings (H_c ~ 600 Oe), while Figure 1b shows the M–H loop of FePt/SiO_2 (H_c > 10 kOe) used in the present work.

Q control in vacuum. The sensitivity of MFM is proportional to the Q factor of the cantilever oscillation, and the typical Q factor in atmosphere is several tens to several hundreds. Under vacuum conditions, however, the Q factor is several thousands to several tens of thousands, and, consequently, a significant improvement in the sensitivity of MFM is expected. On the other hand, a Q factor that is too large may reduce the responsiveness, but both the sensitivity and responsiveness can be maintained by electronic Q control.

Q control in vacuum also improves the stability and resolution of MFM. Under atmospheric conditions, when the probe approaches the sample, the amplitude of the cantilever decreases because of the viscous resistance of air molecules; this results in a change in the phase of the cantilever and a decrease in the Q factor. Furthermore, if the cantilever amplitude is increased, then the Q factor will also decrease because of an increase in the viscous resistance of air molecules. Under vacuum conditions, these effects do not exist, so the probe–sample magnetic interactions can be measured stably with a sufficient accuracy [4]. In addition, the lack of adsorbed water on the sample surface under vacuum conditions means that the probe will not be trapped at the surface, and stable high-resolution observations can be performed. The influence

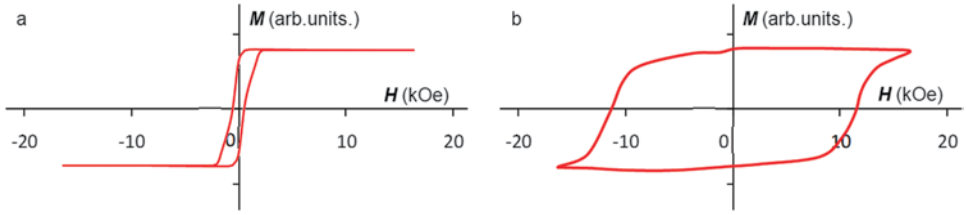

Figure 1: Magnetization–magnetic-field (M–H) loops of (a) CoPtCr (H_c ~ 600 Oe) and (b) FePt (H_c > 10 kOe).

of thermal oxidation or ice coatings can also be reduced when heating or cooling the sample in vacuum.

The experiments were conducted with an AFM5000/AFM5300E (Hitachi High-Tech Science) SPM, and the sample chamber was evacuated to a vacuum level of 10^{-4} Pa by using a turbo-molecular pump. The Q factor in vacuum was controlled to be around 1,500 to 3,000.

Results

MFM of a Nd-Fe-B magnet. Figure 2 shows a comparison of MFM images of a Nd-Fe-B magnet obtained with a conventional Co alloy probe and with the high-coercivity FePt probe. The c-plane Nd-Fe-B sintered magnet was thermally demagnetized, so there should be an even distribution of N and S poles. This means that the MFM signal will be equally divided between attractive and repulsive forces, which will result in an equal amount of bright and dark contrast, respectively, in the images. Figure 2a shows that the conventional Co alloy probe produced an image with a higher amount of bright contrast because the magnetization of the probe was affected by the stray magnetic field of the sample. The attractive force signal was dominant owing to the low coercivity of the probe. However, Figure 2d shows that the high-coercivity FePt probe produces an MFM image with evenly divided contrast and a typical maze-like domain pattern. This indicates that accurate MFM images can be obtained, even when the sample has a strong stray magnetic field like that of a permanent magnet.

Durability of the high-coercivity FePt probe. There is a demand from both academia and industry for high-temperature magnetic domain observations of permanent magnets to determine the coercivity mechanism. This demand is driven by the development of Dy-free permanent magnets that can endure high temperatures of 200 °C for use in electric vehicles. High-temperature magnetic domain observations of Nd-Fe-B magnets using spin-polarized scanning electron microscopy and Kerr effect microscopy have recently been reported [9, 10], but to date there have been almost no reports of correctly performed high-temperature magnetic domain observations of Nd-Fe-B magnets using MFM. To work toward the goal of accurate high-temperature measurements, MFM observations of a high-coercivity FePt film were performed using the high-coercivity FePt probe while the sample was heated to high temperatures (up to 300 °C) in vacuum. The MFM images in Figure 3 reveal that a large number of uniform magnetic domains around 50 nm in size were observed in samples heated between 30 °C and 240 °C. At temperatures higher than 270 °C, the magnetic domains became larger, and at 300 °C, the domains were less distinct. This suggests that the magnetic domain structure of the FePt film changed as the temperature of the film increased. Furthermore, Figure 3 indicates that vacuum MFM with a high-coercivity FePt probe is applicable for temperatures up to 240 °C.

High-temperature MFM measurements in vacuum and atmosphere. Because the surface of a Nd-Fe-B permanent magnet is easily oxidized, it is necessary to consider the influence of thermal oxidation on MFM measurements in high-temperature environments. Figure 4 shows MFM images of a magnetized hot-deformed c-plane Nd-Fe-B magnet obtained with the high-coercivity FePt probe for the following cases: (a) room temperature in vacuum, (b) heating to 150 °C in vacuum followed by an *in situ* MFM observation, and (c) introduction of a small amount of atmospheric gas while maintaining a temperature of 150 °C inside the chamber followed by MFM observation under vacuum conditions. In each case, the same area in the sample is imaged (as identified by powder demarcation and polished crack features).

The dark contrast in the MFM image in Figure 4a indicates an overall magnetic repulsive force between the probe and sample. Because the MFM tip was magnetized to the S pole, the sample surface also had an S-pole magnetization. After the sample was heated in vacuum, there was little change in the topographic image, but the MFM image was brighter than the room-temperature MFM image. This is a result of a temperature-induced reversal in the magnetization of the crystal domains (Figure 4b). When the sample surface was exposed to atmospheric gas at 150 °C, there was a significant change in the topography owing to the influence of thermal oxidation, and the corresponding MFM image did not exhibit any features related to magnetic domains of permanent magnets (Figure 4c).

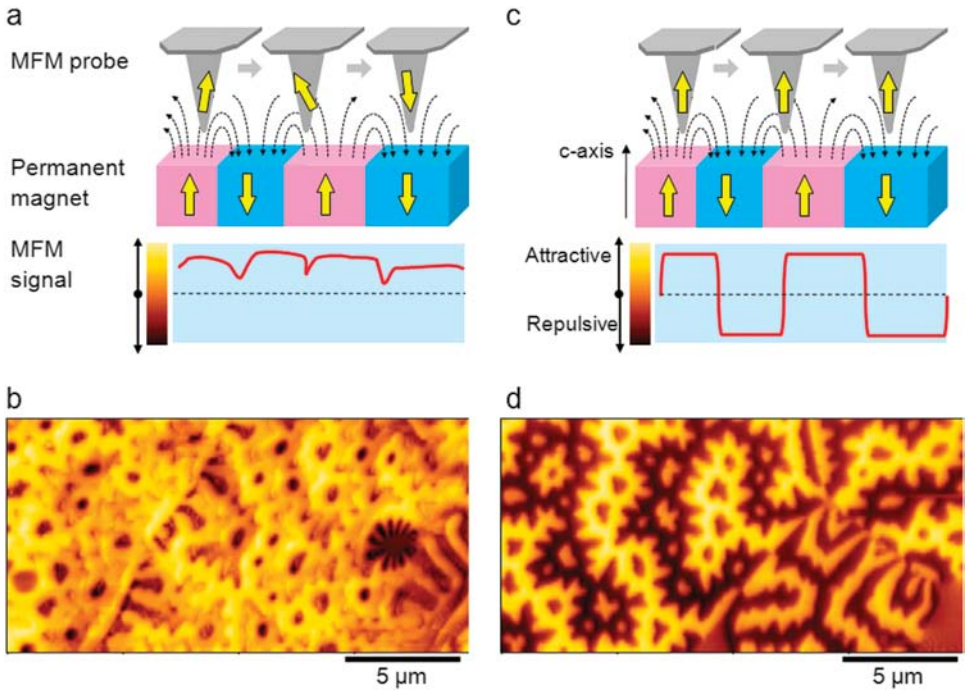

Figure 2: Schematic diagrams of the signal detection and corresponding MFM results of a Nd-Fe-B sintered magnet obtained with a (a, b) CoPtCr (H_c ~ 650 Oe) probe and (c, d) FePt (H_c >10 kOe) probe.

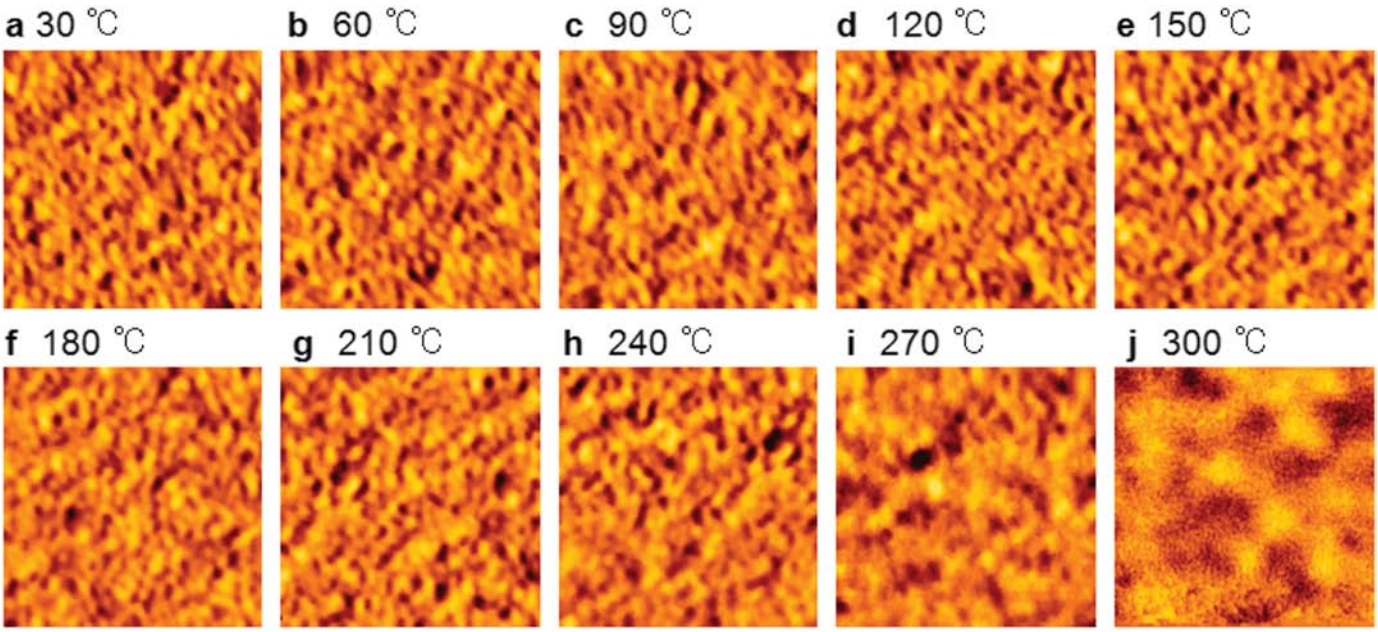

Figure 3: MFM images of a FePt film heated in vacuum obtained using a FePt probe.

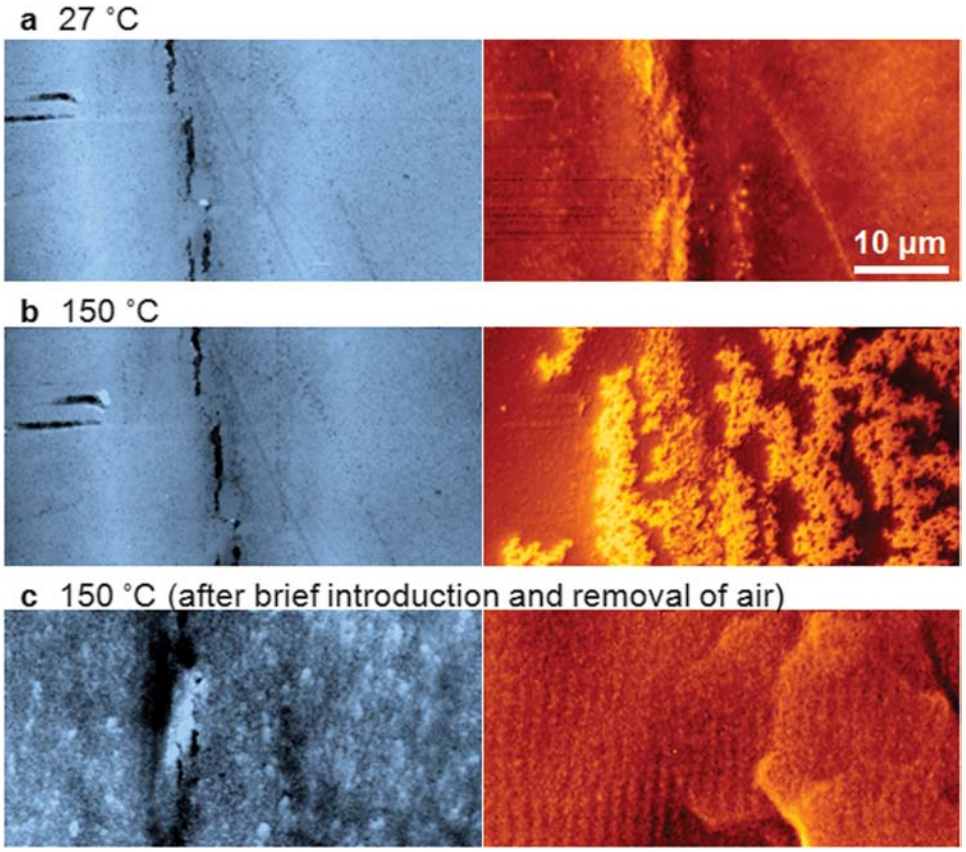

Figure 4: Topographic (left) and MFM (right) images of the same area in a hot-deformed Nd-Fe-B magnet examined in a vacuum of 10^{-4} Pa. (a) 27°C, (b) 150°C, and (c) 150°C after momentary introduction and removal of atmosphere.

***In situ* thermal demagnetization of a sintered Nd-Fe-B magnet.** Figure 5 shows *in situ* MFM images of the thermal demagnetization of a magnetized (N pole) c-plane Nd-Fe-B anisotropic sintered magnet for temperatures up to 200 °C. The measurement was performed with the high-coercivity FePt probe in vacuum (10^{-4} Pa), and the Q factor was controlled to be around 1,500.

Nd-Fe-B sintered magnets usually consist of crystal grains ranging in size from 3 to 10 µm. Even for magnetized samples in large magnetic fields (~50 kOe) exceeding the saturation magnetic field, not all of the crystal grains will be of a single magnetic domain with a magnetization aligned with the external magnetic field. Some crystal grains will be in a maze-like multiple magnetic domain state, as can be seen in the MFM image obtained at 67 °C (Figure 5a). Figures 5b to 5e show the effects of heating the sample to 200 °C, and we see that there is an increase in the number of crystal grains that are in a multiple magnetic domain state as the temperature increases. Furthermore, there are also changes in the maze-like domain pattern in these grains.

The crystal grain boundaries obtained from topographic images are shown together with the MFM images in Figures 5f to 5j, and the magnetization state of each crystal grain is shown by the color coding in Figures 5k to 5o. Grains colored white (I) are in a single-domain state, while those colored yellow (II) are in a multidomain state. Grains that change from being in a single-domain state to a

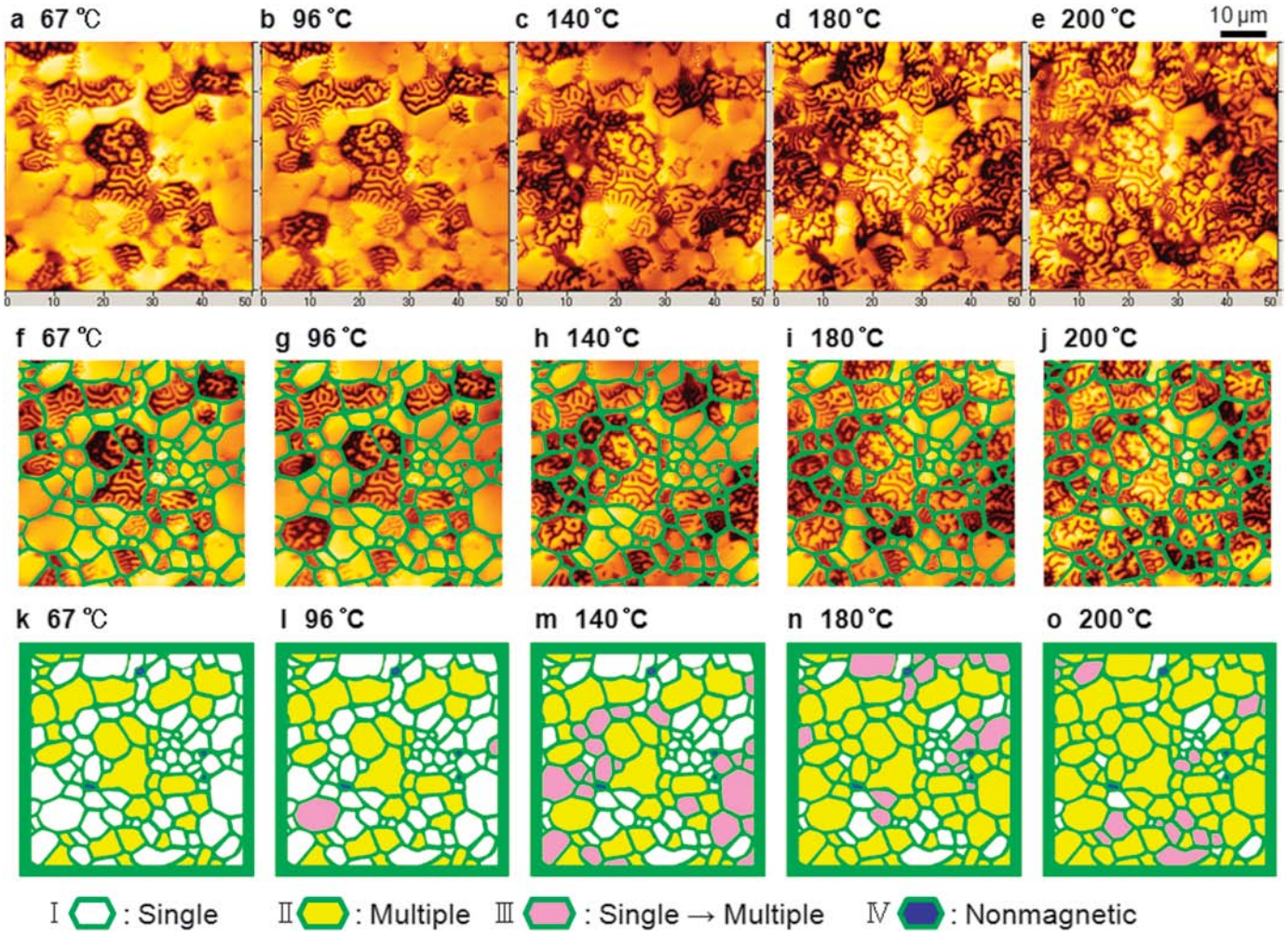

Figure 5: (a–e) MFM images (50 μm) of the thermal demagnetization of a sintered Nd-Fe-B magnet. (f–j) Images in (a–e) showing the grain boundaries. (k–o) Color-coded magnetic domain states.

multidomain state at the noted temperature are colored pink (III). Nonmagnetic (Nd-rich phase) crystal grains are colored blue (IV). Several of the grains that undergo a state change (type III) are adjoined. This phenomenon can be explained as follows. If one crystal grain changes into a multidomain state, then the alignment in the magnetization is lost, and the magnetic field in the crystal grain becomes zero. Adjoining crystals will be affected by this large change in the magnetic field and undergo the same change, thus resulting in a spreading of multiple magnetic domain structures.

Thermal demagnetization of a hot-deformed Nd-Fe-B magnet. Figure 6 shows MFM images of the thermal demagnetization of a magnetized (N pole) hot-deformed c-plane Nd-Fe-B magnet under vacuum conditions (the MFM tip was also magnetized to the N pole; thus, dark contrast should be dominant). The topographic image in Figure 6a shows the center (region A) and boundary (region B) of the hot-deformed magnet powder. The crystals of the hot-deformed magnet powder are finer than those in a sintered magnet, and the flat crystals, ~300 nm in diameter and ~50 nm in thickness [11]. The topographic and MFM images obtained at 30, 70, 100, 130 160, and 200 °C were overlaid and are shown in Figures 6c to 6h. At 30 °C, the magnetization of some crystals has already reversed, as indicated by the bright areas. The images show that areas of reversed magnetization spread from these initial areas as the temperature increases.

The results in Figure 3 showed that *in situ* observations at temperatures higher that 240 °C were difficult, and so for higher-temperature measurements, samples were measured at 30 °C after heating the sample to 300 or 400 °C and maintaining this temperature for 10 minutes (Figures 6i to 6j). The MFM image (Figure 6j) of the sample heated to 400 °C, which is above the Curie point, reveals the complete thermal demagnetization of the sample, as evidenced by the maze-like pattern with an equal distribution of bright and dark contrast. Furthermore, the magnetic domain structure near the center of the powder (region A) is rough, whereas that near the boundary (region B) is finer (Figures 6k and 6l). The topographic images reveal that crystal grains in region A are fine and that those in region B are coarse. It can be concluded that the fine crystal grains near the center have a mostly single magnetic domain structure, whereas the coarse crystal grains close to the boundary have a multiple magnetic domain structure. These crystal grain and magnetic domain

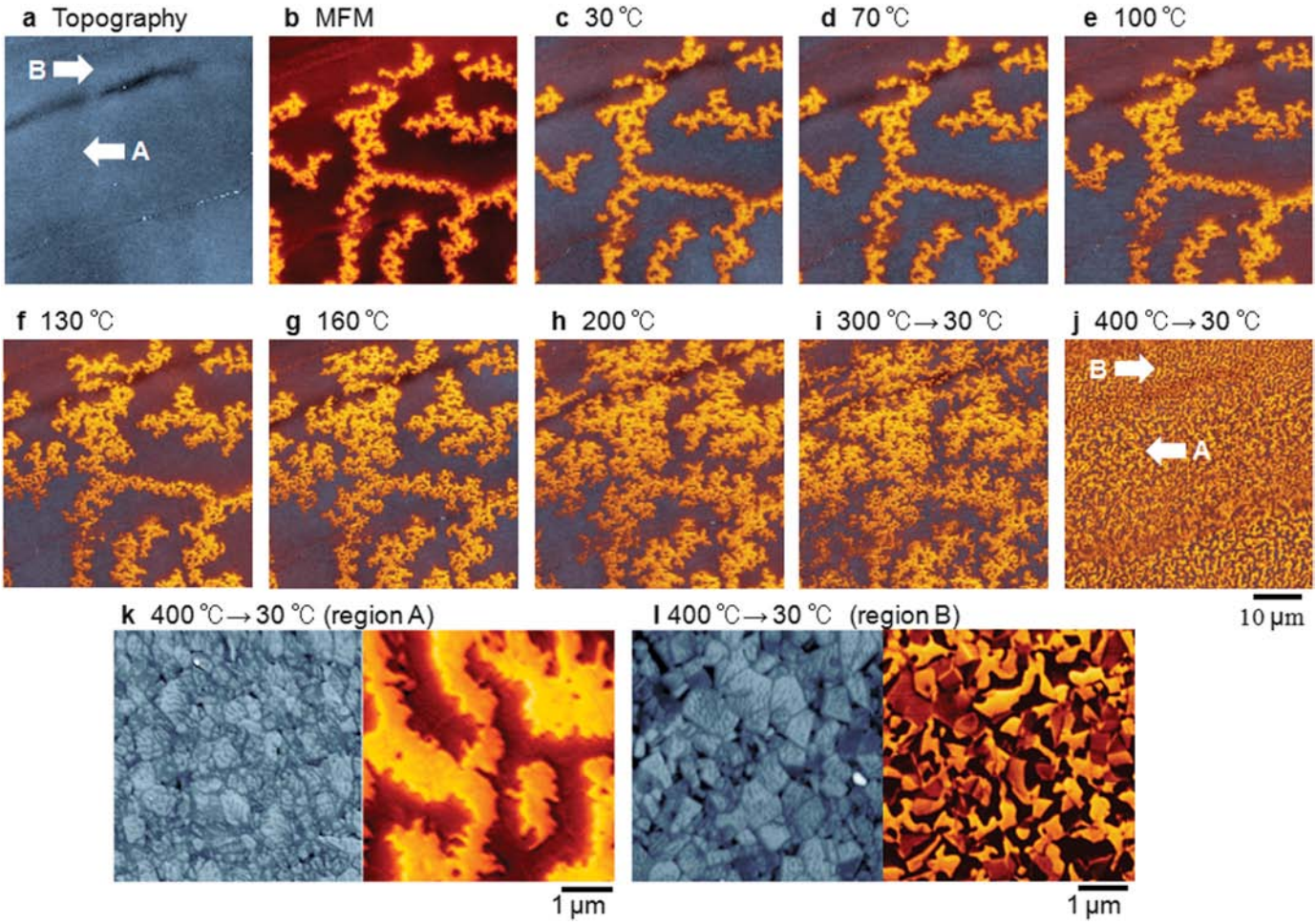

Figure 6: (a, b) MFM images (50 μm) of a magnetized hot-deformed Nd-Fe-B magnet. (c) Overlay image of (a) and (b). (d–j) MFM images of the thermal demagnetization. MFM images (5 μm) of the thermally demagnetized state in (k) region A and (l) region B.

regions are closely related to the specific first magnetization process of hot-deformed magnets [11, 12].

Conclusion

It has been demonstrated that accurate magnetic domain observations of permanent Nd-Fe-B magnets can be performed using a high-coercivity MFM probe and Q control in vacuum. This work has provided a solution to the problem of the stray magnetic field of the sample disturbing the magnetization of the MFM probe. Furthermore, observations of the thermal demagnetization of a Nd-Fe-B magnet to temperatures of up to 400 °C were successful. Microscopic mechanisms such as the diffusion of multi-magnetic domain structures and magnetization inversion were discussed.

Acknowledgments

We would like to thank Profs. H. Saito, S. Yoshimura, and S. Ishio at Akita University for useful discussions on high-coercivity MFM probes and Dr. K. Hioki at Daido Steel Co., Ltd., for valuable discussions and the offer of permanent magnet samples. We are also grateful to Prof. K. Kobayashi at the Shizuoka Institute of Science and Technology and Dr. H. Yamamoto at KRI, Inc., for helpful suggestions on the magnetic domain structures of permanent magnets.

References

[1] Y Martin and HK Wickramasinghe, *Appl Phys Lett* 50 (1987) 1455–57.
[2] E Saitoh et al., *Nature* 432 (2004) 203–06.
[3] T Yamaoka et al., *Jpn J Appl Phys* 45 (2006) 2230–33.
[4] T Yamaoka et al., *J Magn Soc Jpn* 27 (2003) 429–33.
[5] T Yamaoka et al., *IEEE Trans Magn* 41 (2005) 3733–35.
[6] T Yamaoka et al., presentation at 2nd International Symposium on Advanced Magnetic Materials and Applications (ISAMMA 2010), Sendai, Japan, 2010, session CY-03.
[7] T Yamaoka et al., *J Magn Soc Jpn* 35 (2011) 60–66.
[8] A Ito et al., presentation at 31st Annual Conference on Magnetics in Japan, Tokyo, 2007, session 14aE-10.
[9] T Kohashi and K Motai. presentation at the 17th International Microscopy Congress, Rio de Janeiro, 2010, session M6.12.
[10] M Takezawa et al., *J Appl Phys* 115 (2014) 17A733.
[11] K Hioki et al., *Proc. 22nd Int. Workshop on Rare-Earth Permanent Magnets and their Applications* (REPM'12) (2012) 89.
[12] K Hioki et al., presentation at Intermag Europe 2014, Dresden, Germany, 2014, session BC-1.

MT

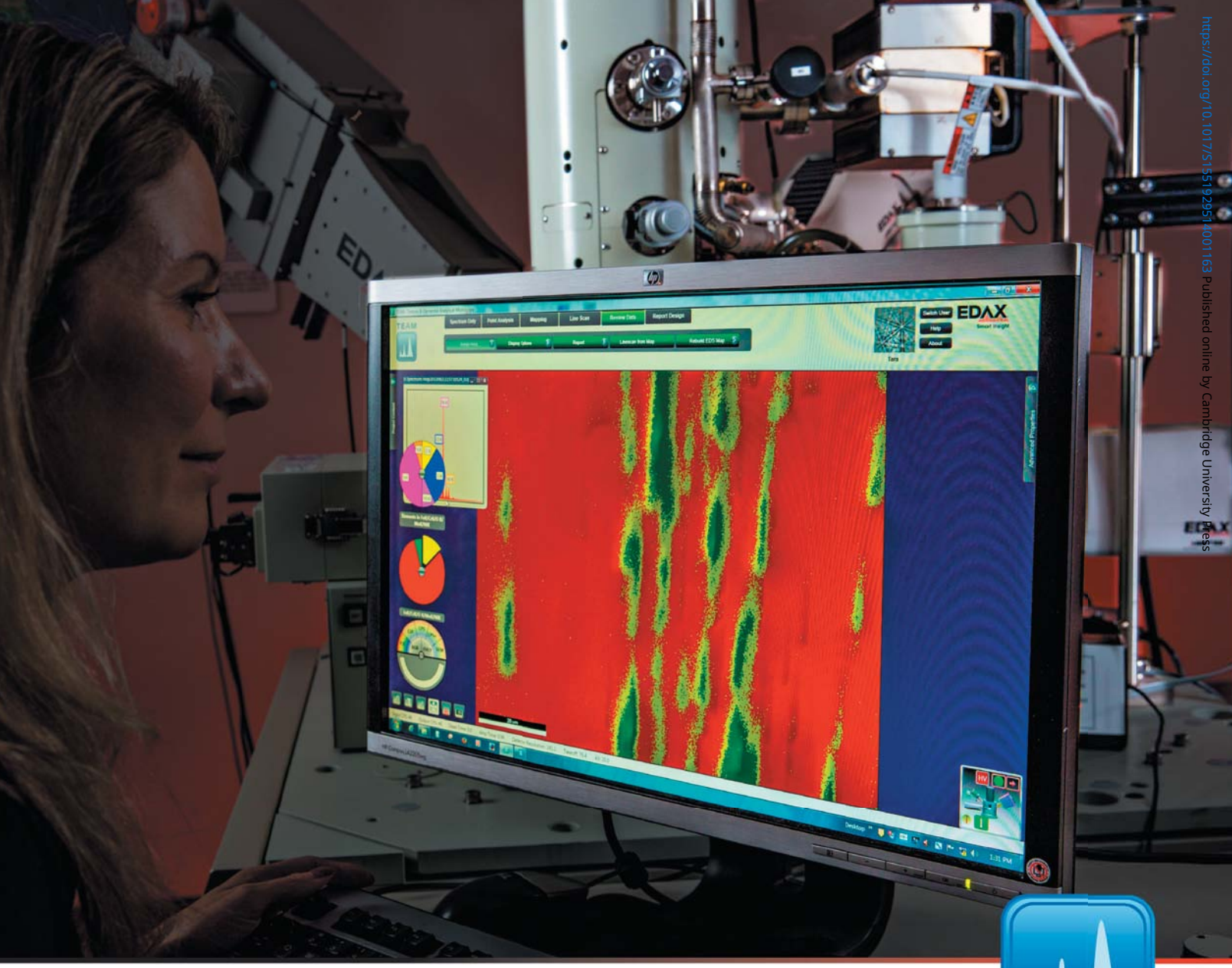

https://doi.org/10.1017/S1551929514001163 Published online by Cambridge University Press